Biomedical Engineering Advances 8 (2024) 100130

Contents lists available at ScienceDirect

Biomedical Engineering Advances

journal homepage: www.journals.elsevier.com/biomedical-engineering-advances

Leaflet stresses during crimping simulations of a CoreValve Evolut Pro model using a compression loading system

Oguz C. Eren [a,b,*], Neil W. Bressloff [b]

[a] Institute of Medical and Biological Engineering, University of Leeds, Woodhouse Ln, Leeds, LS2 9JT, United Kingdom
[b] School of Mechanical Engineering, University of Leeds, Woodhouse Ln, Leeds, LS2 9JT, United Kingdom

ARTICLE INFO

Keywords:
Prosthetic heart valve
TAVI
FEA
CoreValve
Valve durability
Leaflet stress
Crimping method
CLS

ABSTRACT

Background: Transcatheter aortic valve implantation is experiencing continued growth as an option for the treatment of aortic stenosis. With larger numbers of procedures being performed on lower risk and younger patients, there is increased scrutiny on valve durability. Leaflet stresses and potential damage have a significant role to play in this regard. Predictions of leaflet stresses have so far focused on either fluid-structure interaction simulations of blood flow through the prosthesis or, crimping simulations using a cylindrical surface. However, in reality, when a compression loading system (CLS) is used in the crimping of self-expanding valves, this could result in different stresses in the valve leaflets relative to those that might occur in crimping with a cylindrical surface.

Method: A full model of a CoreValve Evolut Pro (Medtronic, Minneapolis, MN, USA) device was developed, comprising the frame, skirt and leaflets along with a representative model for the CLS as used in clinical practice. The full device was crimped to a final diameter of 18 Fr using the CLS model and the distribution and intensity of leaflet stresses was assessed. A similar assessment of leaflet stresses was also performed for crimping using radial displacement of a cylindrical surface. Comparison of the predicted leaflet stresses between the two models was undertaken, alongside a comparison of the stresses produced when dynamically loading the leaflets after deployment of the valve.

Results: Both the CLS and cylinder crimping methods produced higher average and peak stresses on the leaflets compared to those produced during leaflet loading. The peak von Mises stresses for CLS crimping, cylinder crimping, and leaflet loading were 3.42 MPa, 3.92 MPa, and 1.77 MPa respectively. The leaflet folding pattern between the CLS crimping and cylinder crimping methods were different, resulting in different high stress locations on the leaflets. However, the average stress magnitude at the final crimped stage between the two crimping methods were similar.

Conclusions: High fidelity simulations of crimping and expansion of a complete CoreValve Evolut Pro model using a compression loading system model have been performed, wherein the results showed that peak leaflet stresses in the crimped valve were approximately twice as high as the maximum leaflet stresses under dynamic loading. This finding has significant implications for device durability due to the high stresses and possible damage they might inflict on the leaflets. It was also found that crimping using a compression loading system versus a simpler cylindrical surface produced different folding patterns and stress distributions. However, for future studies that are not concerned with accurately capturing the leaflet folding patterns and stresses throughout the crimping process, crimping via a cylindrical surface can be used instead of simulating the full CLS model.

1. Introduction

Valvular heart disease is a growing global health concern, currently estimated to affect 50 million people worldwide [1]. Among the four valves of the heart, the high pressure environment of the aortic valve makes it particularly prone to valve disease through stress related dysfunction. This dysfunction is mainly caused by the calcification of the valve leaflets resulting in the narrowing of the aortic valve annulus,

* Corresponding author.
E-mail address: o.c.eren@leeds.ac.uk (O.C. Eren).

https://doi.org/10.1016/j.bea.2024.100130
Received 30 January 2024; Received in revised form 5 June 2024; Accepted 10 June 2024
Available online 11 June 2024

referred to as aortic stenosis (AS). The global prevalence of calcific aortic valve disease has increased steadily over the last three decades [2]. It is estimated that there are nearly 300,000 people currently living with severe AS in the UK, with this number predicted to be doubled by 2046 [3,4]. The mortality rate of patients diagnosed with severe AS is 50% at two years and 97% at 5 years, if left untreated [5].

The treatment of severe AS involves the replacement of the diseased valve with a prosthetic heart valve or implantation of a prosthetic valve inside the native valve. Conventionally, replacement is performed by open heart surgery where the diseased valve is excised and a prosthetic valve is sutured in, aptly named surgical aortic valve replacement (SAVR). Based on recent evidence from comparative, randomised trials, the minimally invasive method of transcatheter aortic valve implantation (TAVI), has been increasingly preferred as a treatment option, even in younger and lower-risk patients. Indeed, the annual volume of TAVI procedures in the US exceeded that of SAVR operations for the first time in 2019, with 72,991 TAVI procedures compared to 57,626 SAVR operations [6]. The trend in the treatment of AS indicates that a further increase in TAVI volumes is likely to occur with the anticipated regulatory approval of TAVI for lower-risk patients. Consequently, increased focus on the durability of these bioprosthetic valves is occurring in advance of the likely need to treat increasing numbers of patients if their first valve degenerates and needs replacing.

The durability of prosthetic valves is associated with the calcification of the prosthetic valve leaflets. The role of mechanical stress on leaflet calcification is increasingly accepted to be significant [7–13]. However, the evidence for this association is mostly based on the positional correlation between calcification patterns produced on degenerated native and surgical prosthetic leaflets, and high stress regions of the leaflets during physiological function [9,11,12,14]. The calcification patterns of TAVI valves, and their correlation between high-stress regions of the leaflets, is currently lacking in the literature, most probably due to the recency of the procedure.

In addition to the stresses induced by dynamic loading during physiological function, TAVI leaflets also experience significant stresses during the crimping procedure. Understanding the leaflet stresses associated with crimping, in addition to physiological loading, is increasingly important due to their possible impact on TAVI valve durability. The leaflet stresses associated with crimping may be significantly greater than the stresses induced during valve opening and closing. Also, the location of high stresses could differ, which may influence the calcification patterns of TAVI valves when compared to their surgical counterparts and native valves. The leaflet stresses associated with the crimping of CoreValve devices is currently an under-researched phenomenon in literature. Thus, the main aim of this research was to investigate the leaflet stresses that occur during crimping and dynamic loading of the leaflets in a model of a 26 mm CoreValve Evolut Pro (Medtronic, Minneapolis, MN, USA) device, focussing particularly on the magnitude and location of high stress locations.

1.1. Computational simulations of CoreValve devices

Computational simulations of the TAVI procedure in the literature have grown in volume alongside the increase in TAVI procedures. These simulations have included both balloon-expandable and self-expanding valves and range from crimping and deployment of the valves to FSI simulations of blood flow through the expanded valve. The simulations involving self-expanding valves are most relevant to the research presented in this article, particularly those using models from the CoreValve family. Crimping simulations of CoreValve devices tended to model only the frame and did not include the skirt or the leaflets present in the real device [15–25]. This was mostly justified by referring to the analysis performed by Bailey et al. which found that the mechanical behaviour of the valve was mostly dominated by the properties of the frame for a balloon-expandable valve [26]. The main aim of the majority of CoreValve simulations has been to assess the deployment of the device in different aortic geometries in terms of coronary obstruction, effective orifice area or other clinically relevant parameters. To that end, the lack of leaflets and skirts were justifiable.

However, to computationally assess leaflet stresses in a prosthetic device, the leaflets need to be modelled. In fact, as the commissures of the CoreValve device are located on a segment of the skirt, a full valve model including the skirt and leaflets is necessary. Some publications that modelled the leaflets and skirt in CoreValve simulations modelled both components as a 2D surface meshed with shell elements [27–30]. While this is less computationally demanding and appropriate for certain investigations, to accurately capture the folding pattern during crimping, the leaflets had to be modelled as 3D parts. Other articles reported using continuum stress elements to model leaflets and skirt, however they added the leaflets and skirt after crimping and expanding the CoreValve frame [31–34]. Kandail et al. included the skirt and leaflets meshed with tetrahedral elements during the crimping of a CoreValve model but only crimped down to a diameter of 15.5 mm [35]. A recent article by Brown et al. reported the crimping of a full CoreValve Evolut R model including the leaflets and skirt with volumetric elements to 17.8 Fr [36]. However, they used an immersed finite element-difference (IFED) model without an explicit contact model defined between the leaflets which would not be suitable in capturing the folding patterns, and hence leaflet stresses, during crimping.

Previously, Bressloff published the crimping of a novel self-expanding frame including the skirt and 3D leaflets to 18 Fr, fully capturing the folding pattern of the leaflets and assessed the leaflet stresses associated with crimping to a clinically relevant diameter for the first time [37]. Bressloff identified the required material properties and thickness of the skirt to successfully complete such a simulation and compared the effect of different leaflet thicknesses on the folding patterns and resultant stresses. The research presented here followed on from his investigation and aimed to achieve crimping, also to 18 Fr, of a full valve model of the CoreValve Evolut Pro device, using a model of the compression loading system (CLS) used in clinical practice, to crimp the complex frame structure with variable radius across its height, further enhancing the detailed fidelity of the simulation. The crimping diameter achieved in most simulations in the literature either have not achieved a crimped diameter of 18 Fr [15,19,27,35] or they have not included the leaflets and/or the skirt [16,23–25,31,32,34,38]. Consequently, the simulations reported here do not appear to have been reported in the literature before.

1.2. Crimping process of CoreValve

The CLS comprises an outflow cone, an inflow cone, and an inflow tube. The steps of the crimping of a CoreValve device using this CLS system was described in the relevant FDA document detailing the instruction for use of the CoreValve system [39]. Briefly, the crimping procedure involves the following sequence: (i) the outflow cone is pushed over the outflow end of the valve, (ii) the inflow tube is pushed over the portion of the valve covered by the outflow cone, (iii) the inflow cone, a funnel-like structure, is pushed over the inflow end of the valve, (iv) the outflow cone and inflow cone are simultaneously pushed over the valve such that the valve is fully within the inflow cone, (v) the inflow tube is pushed over the entirety of the valve, (vi) the crimped valve is pulled within a sheath on the catheter.

As a simpler alternative to the CLS, most computational simulations in the literature, have used a radially constricting cylinder to simulate the crimping of CoreValve [15–18,20,21,24,25,27,28,31–36,38]. This method mimics the crimping process for balloon expandable valves in which a crimping tool applies a radially inward force on the valve. Bosmans et al. have reported crimping by pulling the valve model into a single funnel [19], this being a partial representation of the entire CLS process which includes two cones and a cylindrical tube as described above.

In this research, we wanted to accurately capture the leaflets stresses

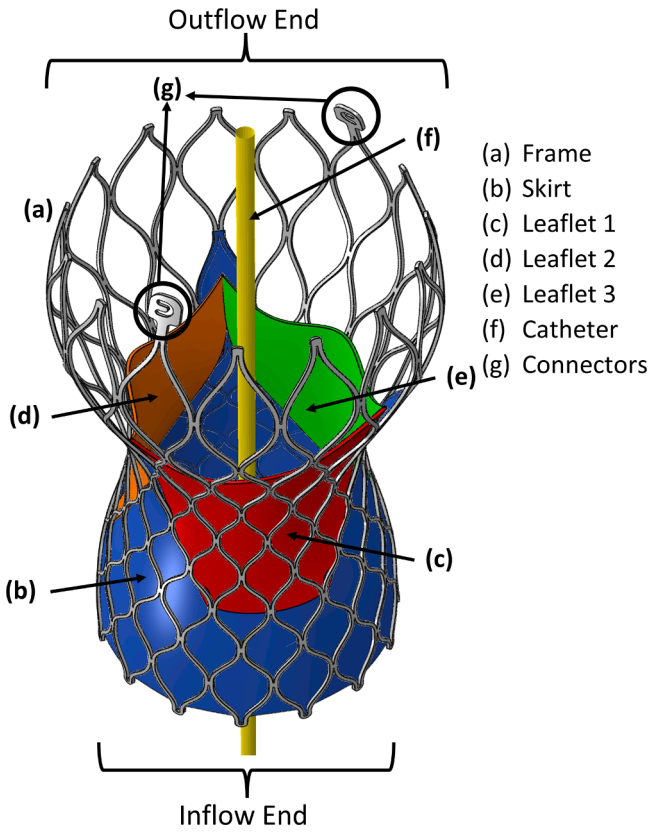

Fig. 1. The full CoreValve Evolut Pro model with the leaflets, skirt, connectors, and the catheter shown. The three leaflets are individually coloured and labelled, with this colour scheme used consistently throughout the article in subsequent images. The inflow and outflow end of the valve is also specified.

Table 1
Nitinol material model parameters [15].

Parameter	Value
E_M (MPa)	47800
E_A (MPa)	51700
ν_M	0.30
ν_A	0.30
ϵ^L	0.063
σ^S_{tL} (MPa)	600
σ^E_{tL} (MPa)	670
σ^S_{tU} (MPa)	288
σ^E_{tU} (MPa)	254
σ^S_{cL} (MPa)	900
T_0	$37^{\circ}C$
$\left(\frac{\delta\sigma}{\delta T}\right)_L$ $(MPaT^{-1})$	6.527
$\left(\frac{\delta\sigma}{\delta T}\right)_U$ $(MPaT^{-1})$	6.527

and folding patterns and to investigate how they compared when crimping using the CLS approach or the radial displacement of a cylindrical surface.

2. Methodology

This section describes the computational model and finite element analysis properties used in this research to achieve the aim of determining the leaflet stresses caused by CoreValve crimping. All parts were modelled using the Grasshopper editor in Rhinoceros 3D version 7 (Robert McNeel & Associates, Seattle, WA, USA) and exported into Abaqus/Explicit R2022 (Simulia, Dassault Systèmes, Providence, RI, USA) where all simulations were performed.

The ARC4 high performance computing cluster at the University of Leeds was used for all simulations. 8-way parallel partitioning of the complete simulation domain was employed in all simulations with 2.0 GHz Intel Xeon Gold 6138 CPUs. All simulations were solved with double precision.

Fig. 1 shows the full model CoreValve Evolut Pro assembly used in this study including the frame, leaflets, skirt, connectors, and catheter. The modelling and material properties of each part is described in the sections below.

2.1. Frame

The frame was modelled from images of the CoreValve Evolut Pro available online and based on dimension data reported in the literature [40–42]. The 26 mm model was chosen as it is the recommended size for the largest selection of aortic valve annuli diameters present in the population [39,43,44]. The connector tabs were also included in the frame model as they are used during the CLS crimping process. The strut width and strut thickness were constant across the height of the frame with values of 0.25 mm and 0.3 mm respectively.

The material model for the frame was modelled using the superelasticity property definition in-built in ABAQUS/Explicit R2022 based on the shape-memory study of superelastic behaviour by Auricchio and Taylor, with parameters specified by Finotello et al. [15,45]. The superelastic model in ABAQUS is based on the uniaxial stress-strain response of phase transforming materials. Nitinol is such a phase transforming material which is in the austenite phase under no loading conditions and starts transforming into martensite beyond a certain stress. Both phases are assumed to follow isotropic linear elasticity. During phase transformation, the elastic properties of the material are calculated from the Young's moduli of austenite and martensite following the rule of mixtures:

$$E = E_A + \zeta(E_M - E_A) \tag{1}$$

$$\nu = \nu_A + \zeta(\nu_M - \nu_A) \tag{2}$$

where ζ is the fraction of martensite, E_A is the Young's modulus of austenite, E_M is the Young's modulus of martensite, ν_a is the Poisson's ratio of austenite, and ν_m is the Poisson's ratio of martensite. After a certain stress, austenite is completely transformed into martensite. On unloading, martensite transforms back into austenite and the transformation strain is fully recovered. The stress at which the reverse transformation occurs is different to the stress at which austenite to martensite transformation occurs. σ^S_{tL} determines the stress at which this transformation begins during loading and σ^E_{tL} determines the stress at which it ends. Similarly, σ^S_{tU} determines the stress at which the phase transformation begins during unloading and σ^E_{tU} determines the stress at which it ends.

The total strain increment, $\Delta\epsilon$ is the sum of the elastic strain increment, $\Delta\epsilon^{el}$, and the increment in transformation strain, $\Delta\epsilon^{tr}$:

$$\Delta\epsilon = \Delta\epsilon^{el} + \Delta\epsilon^{tr} \tag{3}$$

The increment in transformation strain is calculated using the following flow rule:

$$\Delta\epsilon^{tr} = \zeta\frac{\delta G^{tr}}{\delta\sigma} \tag{4}$$

G^{tr} is the transformation flow potential and σ is the stress tensor. The transformation potential is assumed to follow the Drucker-Prager form $G^{tr} = q - p \times \tan\psi$ where p is hydrostatic pressure, ψ is a scaling constant, and $q = \sqrt{\frac{3}{2}S : S}$ is the von Mises equivalent stress. The transformation surface, F^{tr}, also follows the Drucker-Pager form, and varies linearly with temperature, T:

Table 2
Material properties for the valve leaflets, using the hyperelastic Ogden model.

N	μ^i	α^i	D^i
1	0.1591	10.89	0

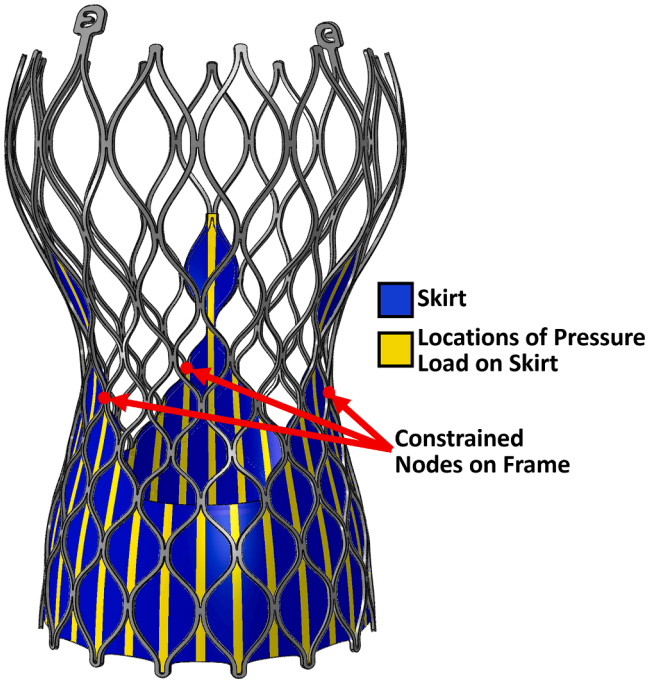

Fig. 2. The nodes on the frame (red) constrained to move only radially and the vertical strips across the skirt (yellow) on which a pressure load of 0.001 MPa was applied. The valve leaflets are not shown in the image for clarity.

$$F^{tr} = q - p \times tan\beta \tag{5}$$

In tensile loading, F^{tr} lies between σ^S_{tL} and σ^E_{tL}; during unloading it lies between σ^S_{tU} and σ^E_{tU}. The angles β and ψ are calculated from tensile and compressive transformation stress levels alongside the uniaxial transformation strain (ϵ^L) which is specified in the material definition. Finally, the variation of the stress levels at which phase transformation takes place are specified for a reference temperature, T_0, and vary linearly according the specified values for the slope of the stress versus temperature curve for loading, $\left(\frac{\delta\sigma}{\delta T}\right)_L$, and the slope for unloading, $\left(\frac{\delta\sigma}{\delta T}\right)_L$.

The parameters used in the simulations in this article for the material properties described above are given in Table 1.

2.2. Skirt

The inner skirt was modelled to fit within 0.05 mm tolerance of the frame across its entire height. The shape of the skirt was based on CoreValve Evolut Pro images online, including the three higher regions culminating in the commissures. The skirt model was built as a surface and not a 3D part. The outer skirt was omitted from the model as it has no interaction with the leaflets during crimping.

The material model for the skirt was based on previous work reported by Bressloff where a PET material model was used [37]. This material definition was similar to that used by Pasta et al. with a Young's modulus of 50 MPa, Poisson's ratio of 0.3 and density of 1.38 g/cm^3 [31].

2.3. Leaflets

The leaflets were modelled in Grasshopper with a thickness of 0.3 mm. The hyperelastic Ogden model was used to define the material properties of the leaflets as described by Bailey et al. and Bressloff [26,37]. The hyperelastic Ogden model describes the strain energy function as:

$$U = \sum_{i=1}^{N} \frac{2\mu_i}{\alpha_i^2}\left(\bar{\lambda}_1^{\alpha i} + \bar{\lambda}_2^{\alpha i} + \bar{\lambda}_3^{\alpha i} - 3\right) + \sum_{i=1}^{N} \frac{1}{D^i}(J^{el} - 1)^{2i} \tag{6}$$

where $\bar{\lambda}_n^{\alpha i}$ are the deviatoric principal stretches, $\bar{\lambda}_i = J^{-\frac{1}{3}}\lambda_i$, λ_i are the principal stretches, N is the strain energy potential order, and μ^i, α^i and D^i are temperature dependant material properties. Table 2 states the values used for these parameters in the simulations in this article.

The density was 1.0 g/cm^3 as used by Bosmans et al. and Bressloff for soft tissues [19,37]. The Ogden model with N=1 shows good agreement with experimental data up to 200% strain in tensile testing [46]. The maximum logarithmic principal strain experienced by the leaflets in this article was 0.460, equivalent to an engineering strain of 58%, well below this limit.

2.4. Catheter

The catheter was modelled as a 3D cylinder with a 1.5 mm diameter and had a fixed position throughout all simulations. The diameter of the catheter was based on physical measurements from an 18 Fr EnVeo PRO delivery system catheter (Medtronic, Minneapolis, MN, USA).

2.5. Constraints

Surface to surface tie constraints were used to model the complete valve. The outer mesh surface of the skirt was tied to the inner surface of the frame. The non-free edges of all three leaflets were tied to the inner mesh surface of the skirt.

2.6. Crimping cylinder

For the crimping simulations with a cylinder, a cylindrical surface part was generated with a diameter of 32.8 mm and placed concentrically with the valve. This diameter was 0.1 mm greater than the largest radius of the frame.

2.6.1. Steps

The cylinder crimping simulations consisted of three steps.

1. Crimp: A radially inward boundary condition on the cylinder part constricted the valve to 18 Fr.
2. Unsheathe: An axial boundary condition on the cylinder uncovered the crimped valve and allowing it to expand.
3. Load: A pressure load of 0.0159 MPa was defined on the aortic side of the leaflets equating to 120 mmHg to close the leaflets, mimicking dynamic loading during diastole [47].

The step duration for all three steps was 0.1 s and mass scaling was used with a target time increment of 1E-7 s. Kinetic energy was maintained below 1% of internal energy throughout the simulation.

2.6.2. Interactions

All contact definitions comprised æhardg contact with the Penalty friction formulation and a friction coefficient of 0.1. Contact was defined between all components of the valve, and between the cylinder and all other parts. Self-contact was defined for all parts except the cylinder.

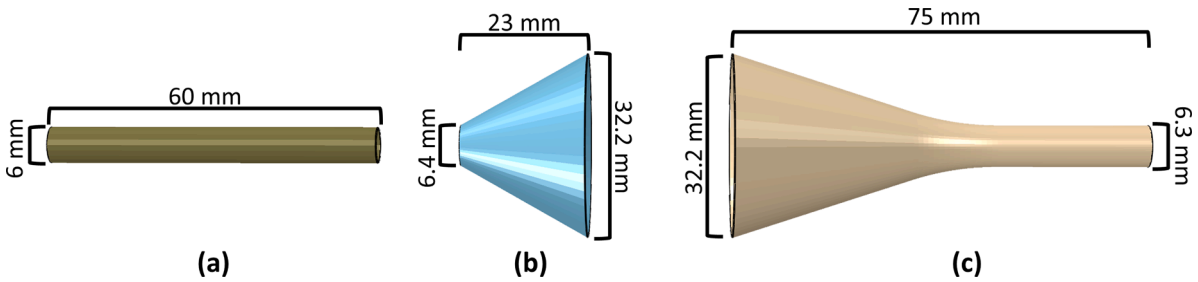

Fig. 3. The Compression Loading System (CLS) model showing relevant dimensions for each part. (a) Inflow Tube, (b) Outflow Cone, (c) Inflow Cone.

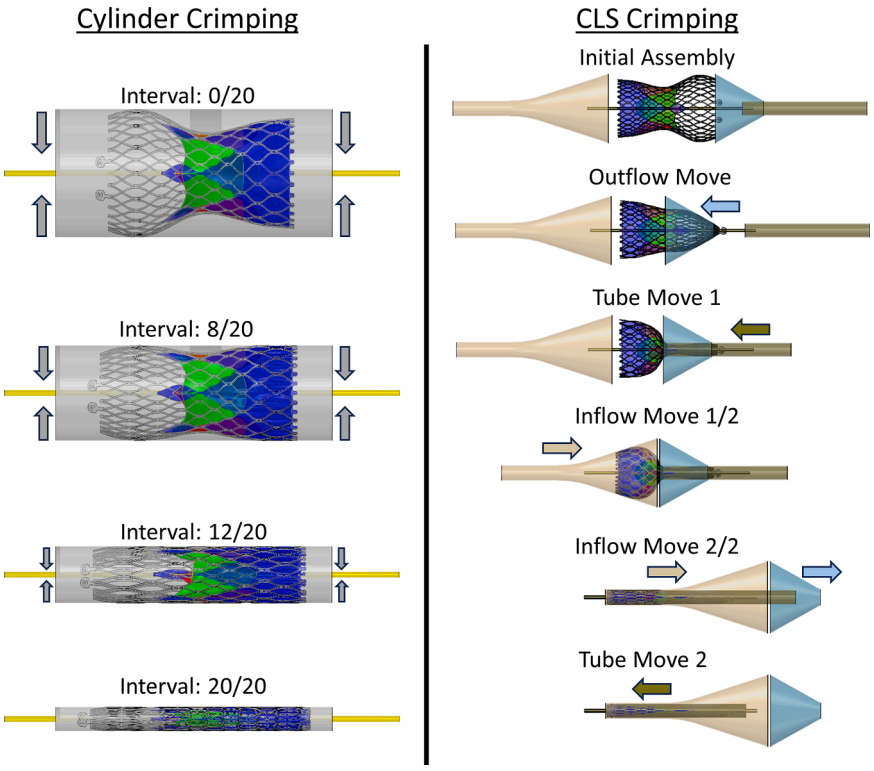

Fig. 4. The steps of the simulation for both cylinder (left) and CLS (right) crimping. The cylinder crimping was performed in a single step, divided into 20 intervals. The images relating to this simulation portray the intervals across this step. The CLS crimping images portray the individual steps across the simulation, with the exception of the Inflow Move step which includes two images for clarity. The arrows on the figure show the direction of the boundary condition for each step/interval, with the arrow colours matching the parts they relate to.

2.6.3. Boundary conditions & loads

The magnitude of the radially inward boundary condition on the cylinder during the Crimp step was 13.3 mm. Three nodes on the middle of the frame across its height were constrained to only move radially to keep the valve in place during crimping and expansion. The position of these nodes is shown in Fig. 2.

The magnitude of the axial boundary condition on the cylinder during the Unsheathe step was 60 mm.

There was a need to apply a pressure load of 0.001 MPa to vertical strips across the height of the skirt to prevent the skirt from pinching between the frame struts and causing deformation errors. The position of these vertical strips is shown in in Fig. 2. The magnitude of this load was determined through iterative simulations where the pressure load was varied from 0.0001 MPa to 0.1 MPa. The chosen value of 0.001 MPa was the lowest magnitude of the tried values that prevented the skirt from pinching between the frame struts.

2.7. Compression loading system (CLS)

The compression loading system (CLS) is a patented part of the CoreValve device which allows for the loading of an expanded CoreValve device onto the dedicated catheter.

Fig. 3 shows the components used to model the CLS system and the associated dimensions. The dimensions were set such that the larger diameter ends of the cones, 32.2 mm, were larger than both the outflow and the inflow end of the valve, which were 32 mm and 26 mm respectively. The inflow tube diameter was set to 18 Fr so as to achieve this final crimped diameter for the valve.

The outflow tube and the outflow cap, which are other components present in the CLS system, were not modelled as these components do not interact with the valve during crimping but are rather used to facilitate engagement between the other CLS components.

2.7.1. Steps

The procedure of crimping a CoreValve using the CLS system was described in the relevant FDA application and briefly summarised in

Table 3
Boundary conditions applied across the CLS crimping simulations. All magnitudes stated within the table are in the axial direction with respect to the valve.

	Outflow Move	Tube Move 1	Inflow Move	Tube Move 2
Outflow Cone	26 mm	0	− 50 mm	0 mm
Inflow Cone	0 mm	0	− 75 mm	0 mm
Inflow Tube	0 mm	37 mm	0 mm	25.4 mm
Frame Connectors	*inactive*	0 mm	*inactive*	*inactive*

Table 4
Element details for all parts used in the simulations.

Part	Element Type	Spacing	Number of Elements
Outflow Cone	C3D8R	1 mm	3,968
Inflow Cone	C3D8R	1 mm	8,256
Inflow Tube	C3D8R	1 mm	1,360
Frame[a]	C3D8R	0.1 mm	198,132
Skirt[b]	S4RS	0.05 mm[c]	714,380
Leaflet[d]	C3D8R	0.1 mm	115,920
Catheter	C3D8R	0.8 mm	2,700
Cylinder	SFM3D4R	1 mm	5,047

[a] Frame elements had second order accuracy and enhanced hourglass control.
[b] Skirt elements had second order accuracy and small membrane strains were used.
[c] For vertical strips across the height of the skirt with the finer mesh, spacing was 0.01 mm.
[d] Leaflet elements had second order accuracy and enhanced hourglass control.

Section 1.2. The steps of the CLS simulations reflected that of the real procedure in terms of the sequential movements of the CLS components. As such, the steps were:

1. Outflow Move: The outflow cone was moved over the outflow end of the valve until the larger end of the cone aligned with the middle of the valve frame.
2. Tube Move: The inflow tube was moved to align with the end of the outflow cone.
3. Inflow Move: The inflow cone was moved over the inflow end of the valve up to the position of the larger end of the outflow cone. This move was divided into two steps in the simulations, something that was found to be necessary to prevent wave speed errors.
4. Tube Move 2: The inflow tube moved axially to cover the entire valve and achieve an 18 Fr crimp.

Fig. 4 shows the steps across the crimping of the valve model with both a cylindrical surface and the CLS system.

The step duration for all steps was 0.1 s. All steps except Tube Move 2 had mass scaling with a target time increment of 4E-7 s, with Tube Move 2 having a target time increment of 2E-7 s. Kinetic energy was maintained below 1% of internal energy throughout the simulation.

2.7.2. Interactions

All contact definitions comprised æhardg contact with the Penalty friction formulation and a friction coefficient of 0.1. Self-contact was defined for all parts. Contact was defined between all valve components and the CLS components. No contact was defined between the CLS components.

2.7.3. Boundary conditions & loads

Three nodes on the middle of the valve frame were constrained to only move radially throughout all steps. Additionally, the connectors, as labelled in Fig. 1, of the valve were kept in place during the first Tube Move step. The magnitude of boundary conditions on the parts in the simulation assembly throughout the steps are shown in Table 3.

Again, a pressure load of 0.001 MPa was applied to regions around the skirt to prevent the skirt pinching in between the frame struts and causing deformation errors.

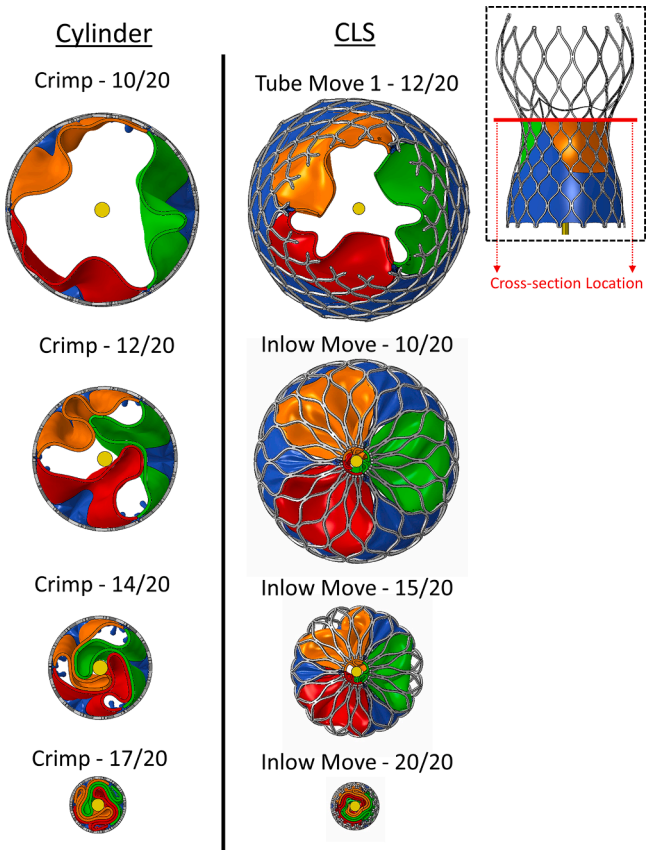

Fig. 5. The folding of the leaflets throughout the simulation for both cylinder (left) and CLS (right) crimping. Each step was divided into 20 intervals and the relevant step and interval for each image is specified above. For visual clarity, each image is from an axial cross-section of the valve, situated 3 mm below the commissures. The position of the axial cross-section across the height of the valve is shown in the top-right image, with respect to the undeformed frame.

2.8. Meshing

The mesh resolution for the frame was based on previous mesh resolution studies across several research groups, including our own, which concluded that three elements across the frame struts in the radial direction ensured mesh independency [15,16,38,48]. The mesh resolution for the skirt was based on previous work by Bressloff regarding the mesh resolution necessary to achieve an 18 Fr crimp diameter with a full valve model [37]. Regions of the skirt that were observed to pinch in between the frame struts were partitioned separately and assigned a finer mesh alongside the pressure load applied on these regions.

Table 4 details the element type and mesh resolutions of all parts across both the crimping cylinder and CLS simulations.

3. Results

Fig. 5 shows the folding of the leaflets across the crimping steps of the valve for both cylinder and CLS crimping. While cylinder crimping uniformly constricts the frame, and hence the leaflets, across the height of the valve, in CLS crimping the diameter of the outflow end on the valve is reduced before the inflow end. This difference can be seen in Fig. 5, particularly in the 10th and 15th interval images for CLS crimping.

Fig. 6 shows the final crimped valve for both the CLS and cylinder crimping simulations across axial cross-sectional slices. The heights of

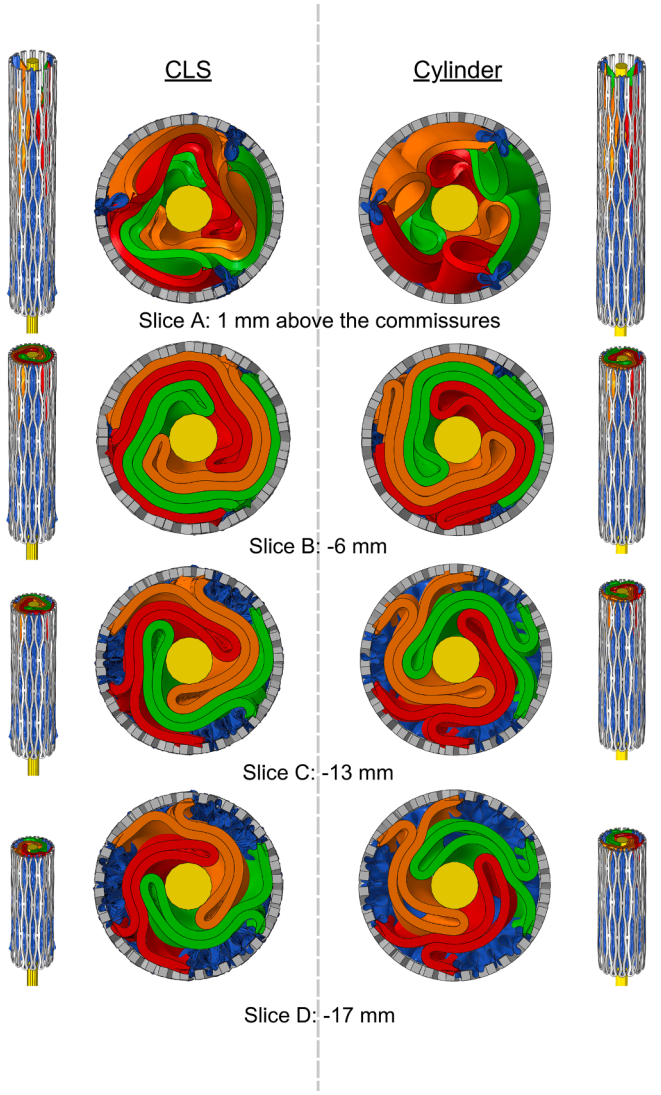

Fig. 6. Planar slices across the height of the crimped valve showing leaflet folding patterns for both cylinder and CLS crimping. Slice A is 1 mm above the leaflet commissures; slice B is 6 mm, slice C 13 mm, and slice D 17 mm below the commissures.

the slices are set to capture the varying leaflet folding patterns across the height of the prosthetic valve. The densest packing in the slices shown, occurred 6 mm below the commissures. This region corresponded to the area across the height of the valve which had the smallest frame diameter whilst holding the largest amount of leaflet material. Note that this did not correspond to the narrowest part of the frame in general, but rather the region with the most amount of leaflet material. Due to the shape of the frame and the leaflets, the other regions across the height of the valve were less packed.

While the initial circumferential orientation of the valve in both the CLS and cylinder crimping cases were the same, the final leaflet folding patterns were significantly different. First, the leaflets folded around the catheter in opposite rotations. In the CLS case, the leaflets wrapped around the catheter in a clockwise direction as seen from the outflow end. In the cylinder case the wrapping occurred in an anti-clockwise manner.

Second, the number of folds also differed between the two crimping simulations. Leaflets in the CLS case only had a single fold while the leaflets in the cylinder case had two. These folds correlated to the higher stress locations shown in Fig. 7, which depicts the stresses at the final crimp diameter for each leaflet in both crimping methods, with the leaflets portrayed in an undeformed state. In Fig. 7, the inner surface of the leaflets relates to the radially inward face, or the ventricular side, and the outer surface relate to the radially outward face, or the aortic side.

All leaflets across both crimping processes exhibited high stress regions around the middle of the leaflet, particularly visible in the inner surface contours. This high stress area corresponded to the main fold which occurred in all leaflets in both CLS and cylinder crimping. This main fold can be seen in the top series of images in Fig. 7, for each individual leaflet, and was located at the portion of the leaflet closest to the catheter. The stress was higher on the inner surface as this face was in tension while the outer face was in compression. The secondary fold which occurred in cylinder crimping, located close to the frame, also produced high stresses which, conversely, are prominently visible on the outer faces. This was because these folds were in the reverse direction where the outer face was in tension and inner face was in compression. The outer surface of the leaflets in CLS crimping also showed high stress regions along the non-free edges of the leaflets, around the leaflet-frame attachment edges. These regions correspond to small kinks that occurred towards the inflow end of the leaflets as can be seen in the CLS slice D in Fig. 6. Broadly, in both crimping methods, higher stresses were present at leaflet-frame attachment edges, and folds. The main difference in leaflet stress contours between the two crimping methods is visible in Fig. 7 where cylinder crimping produced two lines across the faces of the leaflets coinciding with the two folds produced via crimping, whereas CLS crimping only produced one such line.

Fig. 8 shows the leaflet stresses produced after leaflet loading where the valve was closed via the application of a pressure load of 0.0159 MPa. High stresses were observed along the coaptation line of the leaflets, particularly towards the commissures, and at the leaflet-frame attachment edges around each leaflet. High stresses were present on the leaflet-frame attachment edges in both crimping scenarios, as well.

Finally, Fig. 9 compares the average von Mises stresses across all leaflets for each crimping method across all time steps and for closed leaflets following unsheathing of the valve and application of a pressure load equating to 120 mmHg to mimic diastolic loading. As the CLS method constrains the valve in different ways throughout the process, it is important to determine whether higher stresses occur prior to reaching the final crimp diameter. The x-axis of the graph depicts the time through the simulations for cylinder crimping, CLS crimping and leaflet loading. For cylinder crimping, this covers the Crimp step where the cylinder constricts down to 18 Fr. For CLS crimping, this covers the Outflow Move, Tube Move, Inflow Move and Tube Move 2 steps, culminating in the 18 Fr crimping of the valve. For the leaflet loading curve, the x-axis covers the application of the pressure load on the leaflets following the expansion of the valve, culminating with the leaflets fully closed. Although the time duration for each simulation was different, the x-axis of the graph is normalised to align the start and end points of the three curves. The images on the graph portray snapshots from the CLS and cylinder crimping simulations, with their positions on the graph with respect to the x-axis corresponding to the state of the valve at those time increments. The CLS crimping exhibited the higher average stresses overall, with several peaks across the process. The corresponding state of the crimping sequence during these points are also shown in the graph. The movement of the inflow cone over the valve resulted in the highest average stresses caused on the leaflets although this magnitude was only slightly larger than the average stress for the final crimped shape. The average stress on the leaflets throughout cylinder crimping constantly increased until the final crimp diameter. The non-linearity of the average stress curve for the cylinder was most likely caused by the smooth step amplitude curve definition used in the simulations to control the motion of the crimping cylinder where the highest acceleration of this motion occurred around the highest slope of the cylinder average stress curve before the slight plateau. Both crimping methods caused higher average stresses on the leaflets when compared to the leaflet loading.

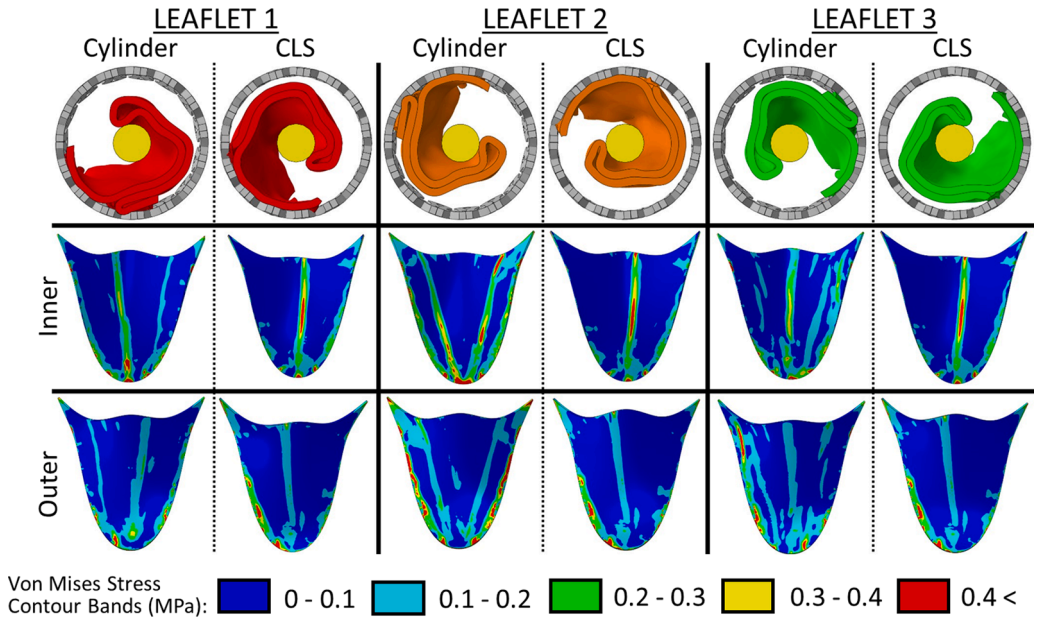

Fig. 7. The final folding pattern of each leaflet for CLS and cylinder crimping and associated von Mises stresses. The top row of images shows the final folded position of each leaflet at 18 Fr, for both the cylinder and CLS cases. Middle row shows the von Mises stress contour of the inner surface (ventricular side) of each leaflet and corresponding crimping method. The bottom row shows the von Mises contours for the outer surface (aortic side) of each leaflet. The contours are shown on an undeformed state for all leaflets. The associated contour colour legend is shown below the figure.

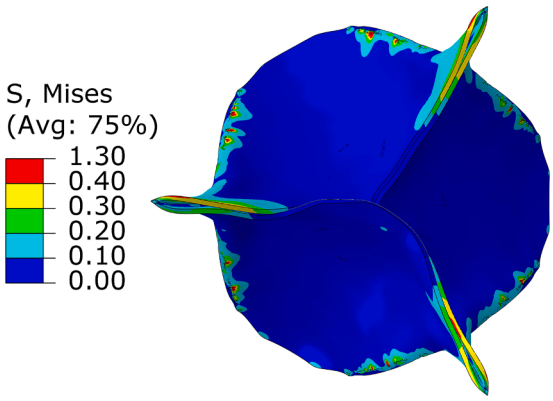

Fig. 8. Contours with a maximum stress limit of 1 MPa showing the von Mises stresses of the three leaflets for leaflet loading with a pressure load of 0.0159 MPa. All three leaflets are shown in the deformed state. The contour colour legend is shown on the left with MPa units.

The peak von Mises stress, across all time steps, was 3.42 MPa for CLS crimping, 3.92 MPa for cylinder crimping, and 1.77 MPa for leaflet loading. These peak values are similar to those reported by Ghosh et al. for leaflet loading as 1.5 MPa at diastole, and Feng et al. for valve crimping as 4.0 MPa at 14 Fr [32,49].

4. Discussion

The main aim of this research was to investigate the leaflet stresses associated with the crimping of a CoreValve Evolut Pro model and how they compared to stresses during leaflet loading. To the authors knowledge this represents the first reported successful simulation of a full CoreValve Evolut Pro model with 3D leaflets crimped to a diameter of 18 Fr. It was also the first simulation to employ a detailed model of the CLS crimping process and to show how this resulted in different folding patterns and stress profiles for the leaflets, relative to the more common approach of using a radially displaced cylindrical surface.

4.1. Leaflet stresses, calcification patterns, and valve deterioration

Calcification of native aortic valve leaflets results in aortic stenosis and can cause the eventual need for the replacement of the valve. The role of mechanical stress on this calcification is increasingly accepted to be significant [7–13]. Originally, calcification of native leaflets was thought to be due to mechanical wear and tear, and hence was exhibited mainly in elderly patients, the fact that not all aging people had calcified leaflets pointed towards a more complex pathophysiology [8,12]. Current consensus describes the calcification of the leaflets as a process with several stages including the initiation of valvular inflammation and its perpetuation due to mechanical stress [8,10]. Calcification initiation points on the leaflets occur due to localised damage to the leaflet microstructure during its physiological function. The inflammatory response to this injury causes calcific deposits on these initiation points which may be propagated across other parts of the leaflets, in particular those areas that experience higher mechanical stress [8]. Hence, leaflet stresses cause the calcification initiation points on the leaflets, with the calcification propagating out from these points across areas of high stresses on the leaflets.

In a landmark article, Thubrikar et al. qualified the different patterns of calcific deposits present on the leaflets of aortic stenosis patients and observed two main modes: the radial pattern where calcification extends radially inward from initiation points on the leaflet attachment edges towards the middle of the leaflet; and the coaptation pattern where calcification occurs along the coaptation line of the leaflets [12]. These two calcification patterns could exist together on the same patient and correlated with the regions of high stress experienced by the valve during physiological loading. This relationship between the calcification initiation points and subsequent propagation locations with the high stress location of the leaflets was further reinforced in several studies. Sturla et al. modelled calcified native leaflets from three explanted human aortic valves and found calcification patterns mostly agreeing with those reported by Thubrikar et al [11]. Halevi et al. also concurred with the calcification patterns found by Thubrikar et al. in their article where they examined scans from 36 native valve leaflets and identified the calcification initiation points by determining the area with the highest density of calcium [9]. Arzani et al. also computationally

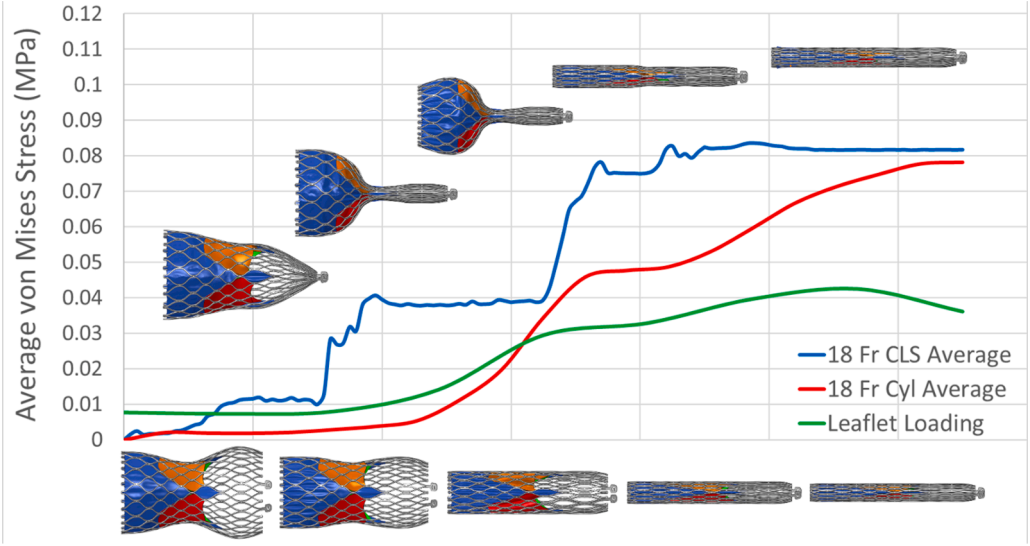

Fig. 9. Average von Mises stress across all leaflets throughout the crimping simulation for both cylinder (red) and CLS (blue) crimping simulations. The average von Mises stress across the leaflets for dynamic loading also shown in graph (green). Side views of the steps of the CLS crimping are shown above, corresponding to, from left to right, the end of the Outflow Move step, the end of the Tube Move step, the midpoint of the Inflow Move step, the end of the Inflow Move step, and the end of the Tube Move 2 step. Side views of throughout the cylinder crimping simulation are shown below the graph, corresponding to, from left to right, frame 4, frame 8, frame 12, frame 16, and the final frame 20.

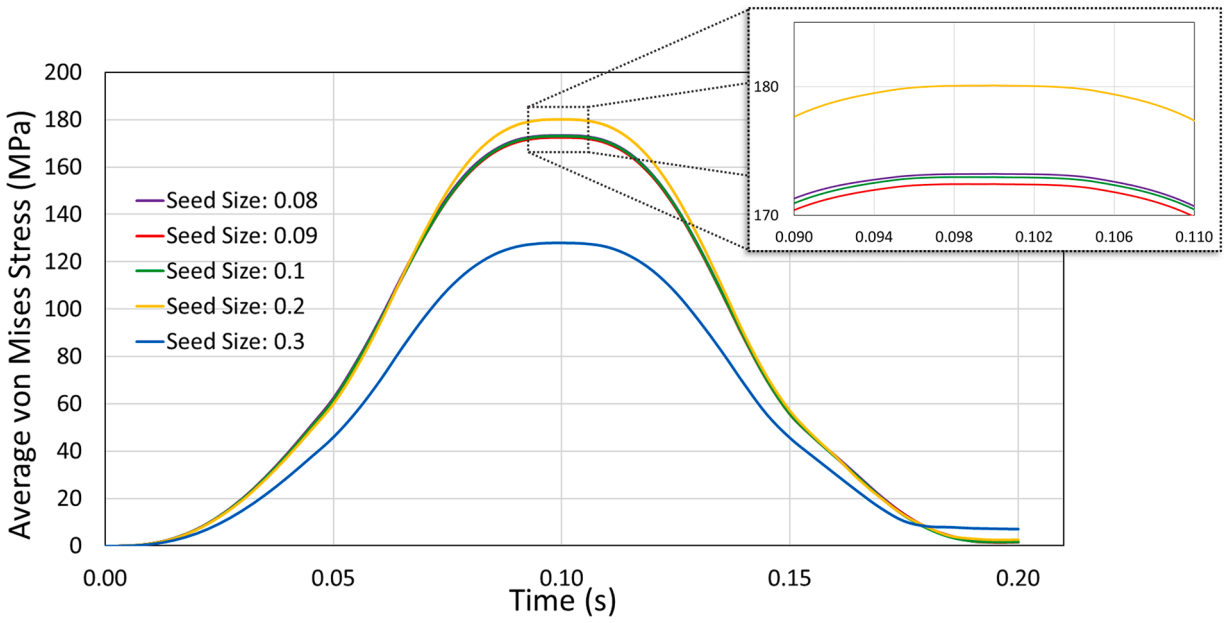

Fig. 10. Average von Mises stress across the frame during 24 mm crimping and expansion for mesh resolutions: (a) 0.08, (b) 0.09, (c) 0.1, (d) 0.2, (e) 0.3.

Table 5
Mesh resolutions used in the mesh refinement study with associated computation time for crimping the frame down to 24 mm diameter.

Global Seed Size (mm)	Number of Elements	Run Time
0.08	403,580	41 hrs 51 min
0.09	240,819	30 hrs 50 min
0.1	198,132	19 hrs 6 min
0.2	51,178	7 hrs 28 min
0.3	8917	2 hrs 20 min

showed that the calcification growth pattern matched the patterns reported by Thubrikar et al. when a calcium initiation point was allowed to propagate along the lines of high strains experienced by a leaflet during opening and closing [7].

The positional alignment between the calcified regions of native aortic leaflets and the high stress regions experienced during valve function evidence the effect of mechanical stress on aortic stenosis. Limited evidence also shows that similar calcification patterns can be found on explanted surgical bioprosthetic valves [14], evidencing the relationship between high stresses on the leaflets and eventual valve deterioration due to leaflet calcification.

4.2. TAVI leaflet stresses

The durability of TAVI valves is under greater scrutiny with the recent trend to lower risk and younger patients being recommended for the procedure. The stresses experienced by the TAVI leaflets are of great

interest due to their association with leaflet calcification. In addition to the stresses induced by dynamic loading during physiological function, TAVI leaflets also experience significant stresses during the crimping procedure.

Several studies have investigated the stresses on CoreValve leaflets during loading through computational simulations. Brown et al. investigated leaflet stresses of a CoreValve Evolut R (Medtronic, Minneapolis, MN, USA) device after deployment during systole and diastole using a fluid-structure interaction, FSI, model and reported peak von Mises stresses of approximately 200 kPa occurring during diastole around the leaflet-frame attachment regions [36]. Qiu et al. applied a diastolic pressure to a CoreValve (Medtronic, Minneapolis, MN, USA) device model with up to 90% under-expansion and up to 90 degrees of pin-wheeling, finding maximum in-plane principal stress values of up to 2 MPa around the commissures and leaflet-frame attachment edges [29]. The non-ideal deployment scenarios increased this maximum stress values and the location of higher stresses extended towards the leaflet free edge. Abbasi et al. generated a model of the CoreValve leaflets based on experimental flow testing of the CoreValve device and reported a maximum in-plane principal stress value of 0.96 MPa located around the leaflet attachment edges and extending radially inward [30]. Luraghi et al. simulated the deployment of a CoreValve Evolut R model into a calcified aortic root followed by FSI simulations with systolic and diastolic flow [27]. They reported a maximum first principal stress of 1.32 MPa which occurred along the coaptation region of the valve leaflets, most likely due to the non-ideal expansion of the valve frame due to the calcification within the aortic root model. A lower peak stress value of 0.89 MPa was also reported for a different aortic calcification pattern, in this case around the leaflet-frame attachment edge. Ghosh et al. also simulated the deployment of a CoreValve Evolut R model within a calcified aortic root and performed a subsequent FSI analysis to determine the hemodynamic behaviour of the leaflets [32]. They reported a maximum von Mises stress of 1.5 MPa (volume-weighted 0.47 MPa) on the leaflets during diastole. Interestingly, the high stress nodes were located both on the leaflet attachment edge, but also along a vertical line in the middle of the leaflet, extending between the middle of the free edge and the bottom of the leaflet, which coincided with the location of high stresses present due to the folds of the leaflets after both cylinder and CLS crimping presented in this article.

Other studies have looked at the stresses associated with TAVI leaflets during crimping, albeit there do not appear to have been any articles published on CoreValve specifically. Alavi et al. crimped a novel self-expanding valve design up to 14 Fr on the bench-top and analysed microscopic damage to the leaflets following expansion, determining that crimping did measurable damage to the leaflets that persisted over time [50]. Feng et al. computationally simulated the crimping of a SAPIEN (Edwards Lifescience, Irvine, CA, USA) device with leaflets up to 12 Fr and found stresses above 4 MPa occurred, primarily around the folds on the leaflets during crimping [49]. Further, Feng et al. recreated the folding of the leaflets in a bench-top experiment and assessed the histology of the leaflets, finding significant tissue damage after folding. Zegdi et al. compared the histology of two SAPIEN valves which had been deployed within a patient before being explanted after a few hours due to complications, with two other SAPIEN valves which had been crimped onto a catheter before the procedure was aborted [51]. They observed similar pathologic microscopic findings in all four valves, concluding that crimping caused significant damage to the leaflets with negligible additional damage caused by balloon expansion. Zareian et al. crimped unique, self-expanding valves with bovine leaflets up to 14 Fr and then exposed the leaflets to a calcifying solution to compare the amount of calcification that would occur against an uncrimped control group [13]. They found that the volume of calcification increased with smaller crimp diameters and that most calcification occurred around the free edges of the leaflets and the leaflet-frame attachment edge.

The higher average and peak stresses compared to leaflet loading seen during the CLS and cylinder crimping might result in micro-structural damage to the leaflets which can influence the durability of the valve. This damage due to crimping was observed by Feng et al., Alavi et al., and Zegdi et al. in their respective publications [49–51]. The location of the high stress regions in Fig. 7, located around the leaflet-frame attachment lines and the middle section of the leaflets, aligned with common calcification patterns observed in degenerating leaflets [12,13]. Particularly, these high stress locations covered the so-called calcification initiation points where the localised damage on the leaflets during crimping could become the starting point of calcification, as described by Halevi et al. [9]. The peak stresses of 3.42 and 3.92 MPa respectively, for CLS and cylinder crimping, were beyond the ultimate tensile strength of human pericardium, which was reported as 2.51 MPa by Lee and Boughner [52]. Further, Feng et al. reported that the threshold for leaflet damage for bovine pericardium leaflets could be as low as 2 MPa based on mechanical loading experiments [49]. These show that the computed stresses during crimping reported in this article can do permanent damage to the leaflet structure, leading to valve deterioration. These findings reiterate the important role the crimping process could have on the eventual calcification of the leaflets.

Although the average and peak stress values for crimping were higher than that of leaflet loading, it is important to note that the valve leaflets undergo cyclic loading for a significantly longer time than crimping. Indeed, most research to date in this area has focused on the mechanics of leaflet opening and closing to evaluate the mechanobiology of valve durability, but greater focus on TAVI valve crimping and the residual structural damage to the leaflets warrants further investigation. With the future possibility of CoreValve devices being delivered to TAVI centres pre-crimped, the implications for the leaflets when being constrained in a compact folded state for a long period of time should be investigated as well.

4.3. *Leaflet folding patterns and CLS crimping*

The leaflet folding pattern in this research greatly affected the magnitude and location of stresses which occur on the leaflets during crimping. This reflected the findings of Bressloff and Feng et al., who both found that the folds and leaflet-frame attachment edges exhibited high stresses during crimping [37,49]. A significant contribution of this work was the simulation of crimping using a model of the CLS system which reflected the reality of the crimping of self-expanding valves in the clinic. Hence, it is worthwhile to assess the merit in simulating the crimping of self-expanding valves using the CLS model rather than a radially displaced cylindrical surface. The location of the leaflet folds was affected by the method of crimping which points towards using the realistic CLS simulations in future research for accurately capturing the leaflet stresses throughout the crimping process, particularly in terms of capturing the high stress locations as a result of the folding patterns. However, the leaflet stresses at the final crimped state were similar between the two processes which implies that it is appropriate to use a radially displaced cylindrical surface for crimping simulations, more generally. It should also be noted here that the crimping method is probably not the only aspect which determines the leaflet folding pattern. The initial orientation of the valve and the initial leaflet positions could also influence the final folding pattern. To our knowledge, there is no current research into what the leaflet folding patterns are in clinical use, and it is likely that each CoreValve Evolut Pro implantation procedure holds a slightly different leaflet folding pattern after crimping due to the different conditions and operators employed. In addition, this research has not compared the simulation of the deployment of a valve following CLS crimping with deployment after cylinder crimping. Valves crimped by the CLS system may exhibit different deployment patterns, particularly in terms of leaflet coaptation after expansion, compared to cylinder crimping which could necessitate the use of CLS crimping in research hoping to accurately capture this.

With crimping diameters getting progressively smaller, the effect of the folding patterns on the leaflets needs to be taken into consideration

as the stresses produced by the crimping process will increase, potentially leading to differing rates of calcification and prosthetic valve durability.

4.4. Limitations

The results presented in this article have been obtained for a model of the CoreValve Evolut Pro device, largely constructed using images available online, which is a major limitation. Currently, no evidence is available to validate the results against an actual device or, indeed, other CoreValve designs. However, the frame designs across the CoreValve generations are very similar, suggesting that the findings presented here could be broadly applicable.

In common with other TAVI crimping simulations, results are dependent on multiple modelling assumptions. These include the neglect of leaflet chemical and fixation treatment and the impact these processes may have on the material properties. Either way, it is noted that material property models are generally approximate. Also, the way constraints and other boundary conditions are defined for securing the leaflets to the frame and skirt could have an impact, particularly on the predicted stresses around these frame-leaflet attachment lines. Further, the contact between the parts was defined as frictionless and the hard contact pressure-overclosure relationship was used. In this contact model the surfaces do not transmit any contact pressure until there is contact between them (i.e. until the clearance between them is zero). The magnitude of contact pressure transmission is limitless when the surfaces are in contact, which may have produced artificially large stresses on the contact surfaces between the frame, cylinder, and CLS parts. However, the hard contact relationship minimizes the penetration between the surfaces in contact which is why this contact method was used. In addition, leaflet loading was simulated as a pressure load on the aortic side of the leaflets rather than an FSI simulation which would more realistically capture the dynamic loading of the leaflets. The leaflet loading was also simulated for a fully and freely expanded valve. In reality, the valve would be expanded into a non-circular aortic root with calcified leaflets around its outer perimeter, under-expanded for anchoring purposes, and prevented from a fully circular expansion. In such a scenario, the leaflet stresses during physiological loading could be greater than reported in this article.

Despite the limitations detailed above, evidence from the research reported in this article suggests that elevated stresses during crimping occur in the vicinity of the attachment edge between the leaflets and the frame, and along the folds that are created in the leaflets. Further, the fact that different folding patterns and leaflet stresses are produced by the CLS and cylindrical crimping, respectively, provides interesting insight and useful guidance for future simulations.

5. Conclusion

In conclusion, this study has presented a description of the full device crimping of a CoreValve Evolut Pro model to 18 Fr, using both a cylindrical surface and a model of the compression loading system. The different folding patterns and associated average von Mises stresses produced by the two methods, showed that the way the crimping procedure is modelled can have an impact on leaflet stresses during crimping. However, there was little difference to the final crimped, average stress values across the crimping methods, a finding which can be used to justify the use of the simpler cylinder crimping method for most future studies, wherein the leaflet stresses across the crimping steps and specific leaflet folding patterns can be neglected. Further, the leaflet stresses produced by both crimping processes were higher than the leaflet stresses during dynamic loading, suggesting that crimping stresses may have a significant effect on device durability.

Declarations

Funding

This research was funded by the University of Leeds. For the purpose of open access, the author has applied a Creative Commons Attribution (CC BY) licence to any Author Accepted Manuscript version arising from this submission.

Data access statement

The data associated with this paper are openly available from the University of Leeds Data Repository. https://doi.org/10.5518/1541

Ethical approval

Not required.

CRediT authorship contribution statement

Oguz C. Eren: Writing – original draft, Visualization, Methodology, Investigation, Conceptualization. **Neil W. Bressloff:** Writing – review & editing, Supervision, Methodology, Investigation, Funding acquisition, Conceptualization.

Declaration of competing interest

The authors declare that they have no known competing financial interests or personal relationships that could have appeared to influence the work reported in this paper.

Acknowledgments

This work was undertaken on ARC4, part of the High Performance Computing facilities at the University of Leeds, UK.

Appendix A. Mesh refinement

The C3D8R elements used to mesh the valve frame and leaflet tend to not be stiff enough during bending. The stresses and strain values for these elements are most accurate in the integration points which are located in the middle of the element. Hence, to accurately capture the stresses across the struts of the frame and the thickness of leaflet, which undergo bending in the crimping simulations, a relatively fine mesh is necessary. A mesh refinement study was undertaken to determine the frame mesh resolution that ensured mesh independecy of the predicted von Mises stresses while minimising computational cost. In this study, the valve frame was crimped via cylinder to 24 mm and then allowed to expand. Fig. 10 shows the average von Mises stress across the valve frame for 5 different mesh resolutions. The global seed size, number of elements, and computational run time of each mesh resolution case is shown in Table 5.

Fig. 10 shows sufficient average von Mises stress conversion beyond a global seed size of 0.1 mm. This mesh resolution agrees with literature data which report that a minimum of 3 elements across the thickness of the frame struts is sufficient to achieve mesh independency in TAVI valve crimping simulations [15,38,53]. Hence, a global seed size of 0.1 mm, which resulted in three elements across the frame thickness while minimising the computational cost, was used in this article.

Supplementary material

Supplementary material associated with this article can be found, in the online version, at 10.1016/j.bea.2024.100130.

References

[1] S. Coffey, R. Roberts-Thomson, A. Brown, J. Carapetis, M. Chen, M. Enriquez-Sarano, L. Zuhlke, B.D. Prendergast, Global epidemiology of valvular heart disease, Nat. Rev. Cardiol. 18 (2021) 853–864, https://doi.org/10.1038/s41569-021-00570-z.

[2] G.A. Roth, G.A. Mensah, C.O. Johnson, G. Addolorato, E. Ammirati, L.M. Baddour, N.C. Barengo, A.Z. Beaton, E.J. Benjamin, C.P. Benziger, A. Bonny, M. Brauer, M. Brodmann, T.J. Cahill, J. Carapetis, A.L. Catapano, S.S. Chugh, L.T. Cooper, J. Coresh, M. Criqui, N. DeCleene, K.A. Eagle, S. Emmons-Bell, V.L. Feigin, J. Fernandez-Sola, G. Fowkes, E. Gakidou, S.M. Grundy, F.J. He, G. Howard, F. Hu, L. Inker, G. Karthikeyan, N. Kassebaum, W. Koroshetz, C. Lavie, D. Lloyd-Jones, H. S. Lu, A. Mirijello, A.M. Temesgen, A. Mokdad, A.E. Moran, P. Muntner, J. Narula, B. Neal, M. Ntsekhe, G.M. de Oliveira, C. Otto, M. Owolabi, M. Pratt, S. Rajagopalan, M. Reitsma, A.L.P. Ribeiro, N. Rigotti, A. Rodgers, C. Sable, S. Shakil, K. Sliwa-Hahnle, B. Stark, J. Sundstrom, P. Timpel, I.M. Tleyjeh, M. Valgimigli, T. Vos, P.K. Whelton, M. Yacoub, L. Zuhlke, C. Murray, V. Fuster, Global burden of cardiovascular diseases and risk factors, 1990–2019 update from the GBD 2019 study, Am. J. Cardiol. 76 (25) (2020) 2982–3021, https://doi.org/10.1016/j.jacc.2020.11.010.

[3] G.A. Strange, S. Stewart, N. Curzen, S. Ray, S. Kendall, P. Braidley, K. Pearce, R. Pessotto, D. Playford, H.H. Gray, Uncovering the treatable burden of severe aortic stenosis in the UK, Open Heart 9 (1) (2022) e001783, https://doi.org/10.1136/openhrt-2021-001783.

[4] J.L. d'Arcy, S. Coffey, M.A. Loudon, A. Kennedy, J. Pearson-Stuttard, J. Birks, E. Frangou, A.J. Farmer, D. Mant, J. Wilson, S.G. Myerson, B.D. Prendergast, Large-scale community echocardiographic screening reveals a major burden of undiagnosed valvular heart disease in older people: the oxVALVE population cohort study, Eur. Heart J. 37 (47) (2016) 3515–3522, https://doi.org/10.1093/eurheartj/ehw229.

[5] P. Lancellotti, J. Magne, R. Dulgheru, M. Clavel, E. Donal, M.A. Vannan, J. Chambers, R. Rosenhek, G. Habib, G. Lloyd, S. Nistri, M. Garbi, S. Marchetta, K. Fattouch, A. Coisne, D. Montaigne, T. Modine, L. Davin, O. Gach, M. Radermacker, S. Liu, L. Gillam, A. Rossi, E. Galli, F. Ilardi, L. Tastet, R. Capoulade, R. Zilberszac, E.M. Vollema, V. Delgado, B.C.a.S. Lafitte, A. Bernard, L.A. Pierard, J.J. Bax, P. Pibarot, C. Oury, Outcomes of patients with asymptomatic aortic stenosis followed up in heart valve clinics, JAMA Cardiol. 3 (11) (2018) 1060–1068, https://doi.org/10.1001/jamacardio.2018.3152.

[6] J.D. Carroll, M.J. Mack, S. Vemulapalli, H.C. Herrmann, T.G. Gleason, G. Hanzel, G.M. Deeb, V.H. Thourani, D.J. Cohen, N. Desai, A.J. Kirtane, S. Fitzgerald, J. Michaels, C. Krohn, F.A. Masoudi, R.G. Brindis, J.E. Bavaria, STS-ACC TVT registry of transcatheter aortic valve replacement, Am. J. Cardiol. 76 (21) (2020) 2492–2516, https://doi.org/10.1016/j.jacc.2020.09.595.

[7] A. Arzani, M.R.K. Mofrad, A strain-based finite element model for calcification progression in aortic valves, J. Biomech. 65 (2017) 216–220, https://doi.org/10.1016/j.jbiomech.2017.10.014.

[8] N.H. Dayawansa, S. Baratchi, K. Peter, Uncoupling the vicious cycle of mechanical stress and inflammation in calcific aortic valve disease, Front. Cardiovasc. Med. 9 (2022) 783543, https://doi.org/10.3389/fcvm.2022.783543.

[9] R. Halevi, A. Hamdan, G. Marom, M. Mega, E. Raanani, R. Haj-Ali, Progressive aortic valve calcification: three-dimensional visualization and biomechanical analysis, J. Biomec. 48 (3) (2015) 489–497, https://doi.org/10.1016/j.jbiomech.2014.12.004.

[10] C.M. Otto, J. Kuusisto, D.D. Reichenbach, A.M. Gown, K.D. O'Brien, Characterization of the early lesion of 'degenerative' valvular aortic stenosis. histological and immunohistochemical studies, Circulation 90 (2) (1994) 844–853, https://doi.org/10.1161/01.cir.90.2.844.

[11] F. Sturla, M. Ronzoni, M. Vitali, A. Dimasi, R. Vismara, G. Preston-Maher, G. Burriesci, E. Votta, A. Redaelli, Impact of different aortic valve calcification patterns on the outcome of transcatheter aortic valve implantation: a finite element study, J. Biomech. 49 (12) (2016) 2520–2530, https://doi.org/10.1016/j.jbiomech.2016.03.036.

[12] M.J. Thubrikar, J. Aouad, S.P. Nolan, Patterns of calcific deposits in operatively excised stenotic or purely regurgitant aortic valves and their relation to mechanical stress, Am. J. Cardiol. 58 (3) (1986) 304–308, https://doi.org/10.1016/0002-9149(86)90067-6.

[13] R. Zareian, J. Tseng, R. Fraser, J. Meganck, M. Kilduff, M. Sarraf, D. Dvir, A. Kheradvar, Effect of stent crimping on calcification of transcatheter aortic valves, Interact. Cardiovasc. Thorac. Surg. 29 (1) (2019) 64–73, https://doi.org/10.1093/icvts/ivz024.

[14] R.F. Siddiqiu, J.R. Abraham, J. Butany, Bioprosthetic heart valves: modes of failure, Histopathology 55 (2) (2009) 135–144, https://doi.org/10.1111/j.1365-2559.2008.03190.x.

[15] A. Finotello, R. Gorla, N. Brambilla, F. Bedogni, F. Auricchio, S. Morganti, Finite element analysis of transcatheter aortic valve implantation: insights on the modelling of self-expandable devices, J. Mech. Behav. Biomed. Mater. 123 (2021) 104772, https://doi.org/10.1016/j.jmbbm.2021.104772.

[16] D. Carbonaro, D. Gallo, U. Morbiducci, A. Audenino, C. Chiastra, In silico biomechanical design of the metal frame of transcatheter aortic valves: multi-objective shape and cross-sectional size optimization, Struct. Multidisc. Optim. 64 (2021) 1825–1842, https://doi.org/10.1007/s00158-021-02944-w.

[17] G.M. Bosi, C. Capelli, M.H. Cheang, N. Delahunty, M. Mullen, A.M. Taylor, S. Schievano, A validated computational framework to predict outcomes in TAVI, Sci. Rep. 10 (2020) 9906, https://doi.org/10.1038/s41598-020-66899-6.

[18] A. Finotello, S. Morganti, F. Auricchio, Finite element analysis of TAVI: impact of native aortic root computational modeling strategies on simulation outcomes, Med. Eng. Phys. 47 (2017) 2–12, https://doi.org/10.1016/j.medengphy.2017.06.045.

[19] B. Bosmans, N. Famaey, E. Verhoelst, J. Bosmans, J.V. Sloten, A validated methodology for patient specific computational modeling of self-expandable transcatheter aortic valve implantation, J. Biomech. 49 (13) (2016) 2824–2830, https://doi.org/10.1016/j.jbiomech.2016.06.024.

[20] G.M. Bosi, C. Capelli, S. Khambadkone, A.M. Taylor, S. Schievano, Patient-specific finite element models to support clinical decisions: a lesson learnt from a case study of percutaneous pulmonary valve implantation, Catheter. Cardiovasc. Interv. 86 (6) (2015) 1120–1130, https://doi.org/10.1002/ccd.25944.

[21] E.A. Ovcharenko, K.U. Klyshnikov, A.E. Yuzhalin, G.V. Savrasov, A.N. Kokov, A. V. Batranin, V.I. Ganyukov, Y.A. Kudryavtseva, Modeling of transcatheter aortic valve replacement: Patient specific vs general approaches based on finite element analysis, Comput. Biol. Med. 69 (2016) 29–36, https://doi.org/10.1016/j.compbiomed.2015.12.001.

[22] S. Tzamtzis, J. Viquerat, J. Yap, M.J. Mullen, G. Burriesci, Numerical analysis of the radial force produced by the medtronic-corevalve and edwards-SAPIEN after transcatheter aortic valve implantation (TAVI), Med. Eng. Phys. 35 (1) (2013) 125–130, https://doi.org/10.1016/j.medengphy.2012.04.009.

[23] S. Barati, N. Fatouraee, M. Nabaei, F. Berti, L. Petrini, F. Migliavacca, J.F.R. Matas, A computational optimization study of a self-expandable transcatheter aortic valve, Comput. Biol. Med. 139 (2021) 104942, https://doi.org/10.1016/j.compbiomed.2021.104942.

[24] F. Nappi, L. Mazzocchi, C. Spadaccio, D. Attias, I. Timofeva, L. Macron, A. Iervolino, S. Morganti, F. Auricchio, Corevalve vs. sapien 3 transcatheter aortic valve replacement: a finite element analysis study, Bioengineering 8 (5) (2021) 52, https://doi.org/10.3390/bioengineering8050052.

[25] G. Rocatello, G. De Santis, S. De Bock, M. De Beule, P. Segers, P. Mortier, Optimization of a transcatheter heart valve frame using patient-specific computer simulation, Cardiovasc. Eng. Tech. 10 (2019) 456–468, https://doi.org/10.1007/s13239-019-00420-7.

[26] J. Bailey, N. Curzen, N.W. Bressloff, Assessing the impact of including leaflets in the simulation of TAVI deployment into a patient-specific aortic root, Comput. Methods Biomech. Biomed. Eng. 19 (7) (2016), https://doi.org/10.1080/10255842.2015.1058928.733–444

[27] G. Luraghi, J.F.R. Matas, M. Beretta, N. Chiozzi, L. Iannetti, F. Migliavacca, The impact of calcification patterns in transcatheter aortic valve performance: a fluid-structure interaction analysis, Comput. Methods Biomech. Biomed. Eng. 24 (4) (2021) 375–383, https://doi.org/10.1080/10255842.2020.1817409.

[28] J. Kusner, G. Luraghi, F. Khodaee, J.F.R. Matas, F. Migliavacca, E.R. Edelman, F. R. Nezami, Understanding TAVR device expansion as it relates to morphology of the bicuspid aortic valve: a simulation study, PLoS ONE 16 (5) (2021) e0251579, https://doi.org/10.1371/journal.pone.0251579.

[29] D. Qiu, A.N. Azadani, Structural analysis of regional transcatheter aortic valve underexpansion and its implications for subclinical leaflet thrombosis, Int. J. Numer. Method Biomed. End. 38 (10) (2022) e3641, https://doi.org/10.1002/cnm.3641.

[30] M. Abbasi, M.S. Barakat, D. Dvir, A.N. Azadani, A non-invasive material characterization framework for bioprosthetic heart valves, Ann. Biomed. Eng. 47 (2019) 97–112, https://doi.org/10.1007/s10439-018-02129-5.

[31] S. Pasta, C. Gandolfo, Computational analysis of self-expanding and balloon-expandable transcatheter heart valves, Biomechanics 1 (1) (2021) 43–52, https://doi.org/10.3390/biomechanics1010004.

[32] R.P. Ghosh, G. Marom, M. Bianchi, K. D'souza, W. Zietak, D. Bluestein, Numerical evaluation of transcatheter aortic valve performance during heart beating and its post-deployment fluidstructure interaction analysis, Biomech. Model. Mechanobiol. 19 (2020) 1725–1740, https://doi.org/10.1007/s10237-020-01304-9.

[33] W. Mao, Q. Wang, S. Kodali, W. Sun, Numerical parametric study of paravalvular leak following a transcatheter aortic valve deployment into a patient-specific aortic root, J. Biomech. Eng. 140 (10) (2018) 101007, https://doi.org/10.1115/1.4040457.

[34] S. Morganti, N. Brambilla, A.S. Petronio, A. Reali, F. Bedogni, F. Auricchio, Prediction of patient-specific post-operative outcomes of TAVI procedure: the impact of the positioning strategy on valve performance, J. Biomech. 49 (12) (2016) 2513–2519, https://doi.org/10.1016/j.jbiomech.2015.10.048.

[35] H.S. Kandail, S.D. Trivedi, A.C. Shaikh, T.K. Bajwa, D.P. O'Hair, A. Jahangir, J. F. LaDisa Jr., Impact of annular and supra-annular corevalve deployment locations on aortic and coronary artery hemodynamics, J. Mech. Behav. Biomed. Mater. 86 (2018) 131–142, https://doi.org/10.1016/j.jmbbm.2018.06.032.

[36] J.A. Brown, J.H. Lee, M.A. Smith, D.R. Wells, A. Barrett, C. Puelz, J.P. Vavalle, B. E. Griffith, Patient-specific immersed finite element-difference model of transcatheter aortic valve replacement, Ann. Biomed. Eng. 51 (2023) 103–116, https://doi.org/10.1007/s10439-022-03047-3.

[37] N.W. Bressloff, Leaflet stresses during full device simulation of crimping to 6 mm in transcatheter aortic valve implantation, TAVI, Cardiovasc. Eng. Technol. 13 (5) (2022) 735–750, https://doi.org/10.1007/s13239-022-00614-6.

[38] M. Bianchi, G.M.R.P. Ghosh, O.M. Rotman, P. Parikh, L. Gruberg, D. Bluestein, Patient-specific simulation of transcatheter aortic valve replacement: impact of deployment options on paravalvular leakage, Biomech. Model. Mechanobiol. 18 (2019) 435–451, https://doi.org/10.1007/s10237-018-1094-8.

[39] M.C. LLC, CoreValve System. Technical Report, U.S. Food and Drug Administration (FDA), 2014.

[40] A. Arshi, S.J. Yakubov, K.L. Stiver, C.E. Sanchez, Overcoming the transcatheter aortic valve replacement achilles heel: coronary re-access, Ann. Cardiothorac. Surg. 9 (6) (2020) 468–477, https://doi.org/10.21037/acs-2020-av-38.
[41] A.M. Kasel, S. Cassese, S. Bleiziffer, M. Amaki, R.T. Hahn, A. Kastrati, P. P. Sengupta, Standardized imaging for aortic annular sizing: implications for transcatheter valve selection, JACC Cardiovasc. Imaging 6 (2) (2013) 249–262, https://doi.org/10.1016/j.jcmg.2012.12.005.
[42] M. Weferling, C.W. Hamm, W. Kim, Percutaneous coronary intervention in transcatheter aortic valve implantation patients: overview and practical management, Front. Cardiovasc. Med. 8 (2021) 653768, https://doi.org/10.3389/fcvm.2021.653768.
[43] S.B. Capps, R.C. Elkins, D.M. Fronk, Body surface area as a predictor of aortic and pulmonary valve diameter, J. Thorac. Cardiovasc. Surg. 119 (5) (2000) 975–982, https://doi.org/10.1016/S0022-5223(00)70092-4.
[44] S. Egron, B. Fujita, L. Gullon, D. Pott, T. Schmitz-Rode, S. Ensminger, U. Steinseifer, Radial force: an underestimated parameter in oversizing transcatheter aortic valve replacement prostheses: in vitro analysis with five commercialized valves, ASAIO J. 64 (4) (2018) 536–543, https://doi.org/10.1097/MAT.0000000000000659.
[45] F. Auricchio, R.L. Taylor, Shape-memory alloys: modelling and numerical simulations of the finite-strain superelastic behavior, Comput. Methods Appl. Mech. Eng. 143 (1-2) (1997) 175–194, https://doi.org/10.1016/S0045-7825(96)01147-4.
[46] B. Kim, S.B. Lee, J. Lee, S. Cho, H. Park, S. Yeom, S.H. Park, A comparison among Neo-Hookean model, Mooney Rivlin model, and Ogden model for chloroprene rubber, Int. J. Precis. Eng. Manuf. 13 (5) (2012) 759–764, https://doi.org/10.1007/s12541-012-0099-y.
[47] H.A. Dwyer, P.B. Matthews, A. Azadani, L. Ge, T.S. Guy, E.E. Tseng, Migration forces of transcatheter aortic valves in patients with noncalcific aortic insufficiency, J. Thorac. Cardiovasc. Surg. 138 (5) (2009) 1227–1233, https://doi.org/10.1016/j.jtcvs.2009.02.057.
[48] O.C. Eren, N. Curzen, N.W. Bressloff, Magnetic retrieval of prosthetic heart valves for redo-TAVI, Med. Eng. Phys. 101 (2022) 103761, https://doi.org/10.1016/j.medengphy.2022.103761.
[49] W. Feng, X. Yang, J. Yao, C. Feng, L. Wang, Y. Fan, Bovine pericardium leaflet damage during transcatheter aortic valve crimping: a study of the mechanisms, Comput. Methods Biomech. Biomed. Eng. 26 (10) (2023) 1140–1149, https://doi.org/10.1080/10255842.2022.2110378.
[50] S.H. Alavi, E.M. Groves, A. Kheradvar, The effects of transcatheter valve crimping on pericardial leaflets, Ann. Thorac. Surg. 97 (4) (2014) 1260–1266, https://doi.org/10.1016/j.athoracsur.2013.11.009.
[51] R. Zegdi, P. Bruneval, D. Blanchard, J. Fabiani, Evidence of leaflet injury during percutaneous aortic valve deployment, Eur. J. Cardiothorac. Surg. 40 (1) (2011) 257–260, https://doi.org/10.1016/j.ejcts.2010.11.010.
[52] J.M. Lee, D.R. Boughner, Mechanical properties of human pericardium: differences in viscoelastic response when compared with canine pericardium, Circ. Res. 57 (3) (1985) 475–481, https://doi.org/10.1161/01.RES.57.3.475.
[53] G. Luraghi, F. Migliavacca, A. Garcia-Gonzalez, C. Chiastra, A. Rossi, D. Cao, G. Stefanini, J.F.R. Matas, On the modeling of patient-specific transcatheter aortic valve replacement: a fluid-structure interaction approach, Cardiovasc. Technol. 10 (3) (2019) 437–455, https://doi.org/10.1007/s13239-019-00427-0.